J. Am. Soc. Mass Spectrom. (2019) 30:1857–1866
DOI: 10.1007/s13361-019-02312-5

FOCUS: HONORING HELMUT SCHWARZ'S ELECTION TO THE NATIONAL ACADEMY OF SCIENCES: RESEARCH ARTICLE

Modulation of Gas-Phase Lithium Cation Basicities by Microsolvation

Konrad Koszinowski, Thomas Auth

Institut für Organische und Biomolekulare Chemie, Universität Göttingen, Tammannstr. 2, 37077, Göttingen, Germany

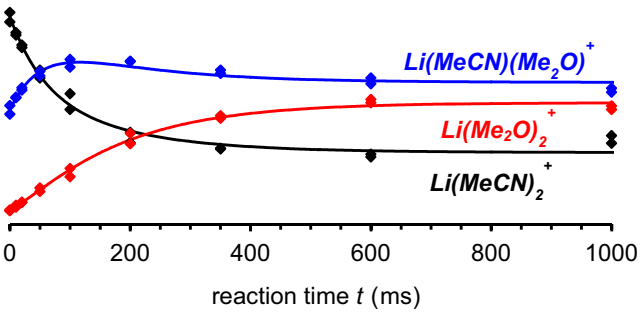

Abstract. In contrast to the extensive knowledge of lithium cation affinities and basicities, the thermochemistry of microsolvated lithium cations is much less explored. Here, we determine the relative stabilities of $Li(A,B)_n^+$ complexes, $n = 2$ and 3, by monitoring their gas-phase reactions with A and B substrate molecules, A/B = Me_2O, Et_2O, tetrahydrofuran, and MeCN, in a three-dimensional quadrupole-ion trap mass spectrometer. Kinetic analysis of the observed ligand displacement reactions affords equilibrium constants, which are then converted into Gibbs reaction energies. In addition, we use high-level quantum chemical calculations to predict the structures and sequential ligand dissociation energies of the homoleptic $Li(A)_n^+$ complexes, $n = 1$–3. As expected, the ligands dissociate more easily from complexes in higher coordination states. However, the very nature of the ligand also matters. Ligands with different steric demands can, thus, invert their relative Li^+ affinities depending on the coordination state of the metal center. This finding shows that microsolvation of Li^+ can result in specific effects, which are not recognized if the analysis takes into account only simple lithium cation affinities and basicities.

Keywords: Ion-molecule reactions, Lithium, Quantum chemical calculations

Received: 28 February 2019/Revised: 12 August 2019/Accepted: 12 August 2019/Published Online: 9 September 2019

Introduction

The smallest alkali metal cation Li^+ plays pivotally important roles in organic and inorganic chemistry, biochemistry, and energy storage alike [1–3]. Despite the extreme diversity of these roles, a common feature of lithium chemistry is given by the strong tendency of Li^+ to interact with Lewis bases, thereby tuning their reactivity or stabilizing supramolecular structures [4–7]. For any understanding of these interactions, their strength must be known. For this reason, there is a high interest in gas-phase lithium cation basicities (LCB), as reflected in numerous experimental and theoretical studies aiming at the determination of these values for a wide range of compounds [8–16]. The LCB of a given molecule A and the related lithium-ion affinity (LCA) [17] are defined as the standard Gibbs reaction energy and the standard reaction enthalpy, respectively, of the dissociation of the complex $Li(A)^+$, Eq. (1).

$$Li(A)^+ \rightarrow Li^+ + A,\ \Delta G_{react}^\circ = LCB(A) \text{ and } \Delta H_{react}^\circ = LCA(A) \quad (1)$$

The deliberate limitation of this approach to mono-ligated Li^+ ions excludes any interference by counter-ion or solvation effects and, thus, renders the systems under consideration perfectly well defined. However, the coordinatively unsaturated character of mono-ligated Li^+ ions also means that these are rather artificial species, which are not encountered in typical environments in the condensed phase. If the trends derived from the analysis of LCBs and LCAs are to be used for the interpretation of condensed phase systems, it is implied that the added complexity, such as the binding of additional ligands, does not qualitatively change the behavior of the lithium ions.

Electronic supplementary material The online version of this article (https://doi.org/10.1007/s13361-019-02312-5) contains supplementary material, which is available to authorized users.

Correspondence to: Konrad Koszinowski;
e-mail: konrad.koszinowski@chemie.uni–goettingen.de

At present, it is not possible to check this assumption because, in marked contrast to the large number of reported LCBs and LCAs, only very few thermochemical data on lithium ions coordinated by more than a single ligand are available. Notable exceptions are the sequential ligand dissociation energies of $Li(H_2O)_n^+$ and $Li(Me_2O)_n^+$, $n \leq 4$, determined by the Kebarle [18] and Armentrout group [19], respectively. A comparison of these values already points to interesting differences. While $LCA(Me_2O) > LCA(H_2O)$ holds for the mono-ligated complexes, the order of the ligand dissociation energies is reversed for the tetra-coordinated ones. This comparison suggests that the coordination of additional ligands can indeed result in qualitative changes of LCBs and LCAs.

Here, we systematically examine the effect of microsolvation on LCBs. To this end, we investigate reversible exchange reactions of the bis-ligated complexes $Li(A)_2^+$, $Li(A)(B)^+$, and $Li(B)_2^+$ as well as of their tris-ligated counterparts $Li(A)_3^+$, $Li(A)_2(B)^+$, $Li(A)(B)_2^+$, and $Li(B)_3^+$, with the neutral substrates A, B = Me_2O, Et_2O, tetrahydrofuran (THF), and MeCN added into the vacuum system of a three-dimensional quadrupole ion trap. From the time profiles of the signal intensities of the ions, we can derive rate constants for the forward and backward reactions, which afford equilibrium constants. These equilibrium constants, in turn, can be easily converted into $\Delta G°$ values corresponding to relative gas-phase basicities of microsolvated Li^+ ions (however, our experiments do not permit the direct determination of absolute thermochemical data). For comparison and for obtaining structural insights, we also perform quantum chemical calculations on the mono-, bis-, and tris-ligated homoleptic complexes $Li(A)^+$, $Li(A)_2^+$, and $Li(A)_3^+$, A = Me_2O, Et_2O, THF, and MeCN. We have chosen this set of ligands because Et_2O, THF, and MeCN all are common solvents used in lithium chemistry and, moreover, we have previously observed complexes of the type $Li(A)_2^+$ and $Li(A)_3^+$, A = Et_2O and THF, upon the analysis of lithium-containing sample solutions by electrospray ionization (ESI) mass spectrometry [20, 21]. We also include Me_2O because in this way we are able to compare our results with those of Armentrout and coworkers [19], which can be used as an absolute anchor point for the relative thermochemical values determined in the present study. Our focus on the homoleptic complexes $Li(A)_n^+$ significantly reduces the number of species to be considered within our quantum chemical investigations, and thus, allows us to perform high-level quantum chemical calculations at justifiable costs. Consequently, our theoretical predictions for the homoleptic complexes promise not only valuable insights at a qualitative level, but also to permit a meaningful quantitative comparison with the experimental results. At the same time, the selected systems fully suffice for the examination of the effects of bound solvent molecules on the LCBs.

Methods

ESI Mass Spectrometry and Gas-Phase Reactivity Studies

For the preparation of microsolvated Li^+ ions, solutions of $LiBPh_4(MeOCH_2CH_2OMe)_3$ or LiCl ($c = 0.1$–1 mM) in Et_2O, THF, or MeCN (≥ 99.5% purity) were injected into the ESI source of an HCT quadrupole-ion trap mass spectrometer (Bruker Daltonik) at a typical flow rate of 8 μL min^{-1}. The ESI source was typically operated with an ESI voltage of − 3000 V and with nitrogen as nebulizer gas (backing pressure of 0.4 bar) as well as drying gas (3 L min^{-1}, $T = 333$ K). The gaseous ions then passed a glass capillary, a skimmer, and two transfer octopoles; the potential differences of which were held low to avoid energetic collisions with residual gas and maximize the signal intensities of microsolvated ions [22, 23]. Subsequently, the ions entered the instrument's actual three-dimensional quadrupole ion trap, which was operated at a trap drive of 40. The observed cations were identified on the basis of their *m/z* ratios, their isotope patterns, and their fragmentation patterns. Ions of interest were mass selected (isolation widths of 1.2–2 u) and subjected to reactions with mixtures of neutral substrates diluted with helium gas ($p_{total} = 6 \times 10^{-4}$ mbar) for variable times *t* (6–11 data points with duplicate measurements in each case) before the recording of mass spectra. In most cases, ligand displacement reactions occurred already during the isolation procedure and, thus, compromised the efficiency of the mass selection, which did not cause serious problems, though. For each combination of two different substrates A and B, two different mixtures and, thus, two different ratios of partial pressures *p*(A) and *p*(B) were applied. In each case, the reactivity of two different parent ions $Li(A)_2^+$ and $Li(A)(B)^+$ was probed, which gave information on the relative stabilities of both the bis- and tris-ligated complexes (see below). Thereby, four independent data sets were obtained for each combination of two different substrates A and B.

The device for preparing well-defined mixtures of neutral substrates and helium has been described previously [24]. It consists of a reservoir (total volume of 2.5 L), which can be evacuated and into which volatile substrates can be added. Me_2O (Sigma Aldrich, 99.9%) was directly added as a gas through an evacuated connection whereas Et_2O, THF, and MeCN (≥ 99.5%) were added as liquids and freed from traces of air by freeze-pump-thaw cycles. After the addition of the substrates into the reservoir, the latter was filled with helium up to a pressure of 6.00 bar. The thus prepared gas mixtures were then fed into the quadrupole ion trap. From the known ratio of substrates in the reservoir and their relative diffusion constants (inversely proportional to the square roots of their molar masses) [25–27], the ratio of their partial pressures in the ion trap can be easily calculated. The known absolute total pressure in the ion trap (see above) then permits the calculation of the partial pressures of the substrates as $p_{substrate} \approx 5 \times 10^{-8}$–$5 \times 10^{-5}$ mbar. In the case of Et_2O, THF, and MeCN, the use of microliter syringes allowed for the straightforward addition of well-defined quantities (1–20 μL, estimated uncertainty due to parallactic deviations and evaporation losses:

< 10%). In the case of Me_2O, we relied on a Pirani gauge (PKR 251, Pfeiffer Vacuum) for measuring its pressure in the reservoir. As we found out, this vacuum gauge displayed a strongly nonlinear response in the sampled pressure range. We calibrated the gauge by monitoring the pressure resulting from the evaporation of measured quantities of liquid Et_2O. Given the close chemical similarity between Me_2O and Et_2O, we assume that this calibration scheme is accurate within a factor of 2.

Data Analysis

For a given experiment at a reaction time t, the Compass DataAnalysis software (Bruker Daltonik) was used to average all recorded scans (so-called weighted average) and to extract the signal intensities of all $Li(A,B)_2^+$ and $Li(A,B)_3^+$ ions. The relatively narrow isolation widths helped to avoid peak overlaps even with imperfect mass resolution and peak shapes. The normalized signal intensities measured at different reaction times t then served as input for kinetic modeling with the Gepasi software package (for the considered kinetic models, see below) [28–30]. Given the large excess of the neutral substrates relative to the ionic complexes, the kinetic modeling affords pseudo-first-order rate constants, from which bimolecular rate constants can be calculated if the partial pressures of the neutral substrates in the ion trap are taken into account. For the present purpose, we were not interested in the absolute bimolecular rate constants themselves, but only in the ratio of the bimolecular rate constants of the forward and backward ligand displacement reaction connecting two complexes, which corresponds to their equilibrium constant K (Scheme 1). Indeed, we could derive robust *ratios* of rate constants of forward and backward reactions, whereas in most cases, the formidable complexity of the examined systems prevented the determination of consistent and meaningful *individual* rate constants from the fitting. Hence, in the following, we will refrain from a detailed discussion of rate constants.

The equilibrium constants K can be easily converted into Gibbs reaction energies $\Delta G°$ values and, thus, into relative gas-phase basicities of microsolvated Li^+ cations according to Eq. (2), with R being the gas constant and T the temperature. The latter (both for the ions and the neutral substrate) has been determined as 300 ± 10 K for three-dimensional quadrupole ion traps [25, 26]. These findings show that the ions in these instruments undergo efficient thermalization. According to the Langevin model [31], the probed ions can be estimated to undergo approx. 80 collisions with He atoms within 10 ms under the given experimental conditions, which confirms the notion that the ions are effectively thermalized before the start of the kinetic experiments.

$$-RT\ln K = \Delta G° \tag{2}$$

For each system, we averaged the ln K values of the four independent data sets [32]. We estimate the uncertainty of the resulting Gibbs reaction energies $\Delta G°$ by adding the standard deviation of the ln K values (statistical component) to the errors introduced by the uncertainties of the substrate ratios and the temperature in the ion trap (systematic component).

$$\begin{array}{ccc} Li(A)_x(B)_y^+ & \underset{k_{backward}}{\overset{k_{forward}}{\rightleftharpoons}} & Li(A)_{x+1}(B)_{y-1}^+ \\ + & & + \\ A & & B \end{array} \qquad K = \frac{k_{forward}}{k_{backward}}$$

Scheme 1. Forward and backward ligand displacement reactions

Quantum Chemical Calculations

All quantum chemical calculations were performed with the software package ORCA 4.0 [33–35] using the *VeryTightSCF* option. The structures of the homoleptic lithium complexes $Li(A)_n^+$ complexes (A = Me_2O, Et_2O, THF, MeCN; $n = 1$–3) and the corresponding ligand molecules were obtained by geometry optimizations with the PBE0 hybrid functional [36] in combination with Grimme's D3 dispersion correction with Becke-Johnson (BJ) damping [37, 38] (*Tight* geometry optimization convergence criteria and large DFT integration grids corresponding to *GRID7* were used). Within these calculations, def2-TZVP basis sets [39] were employed for all elements following the general recommendation of Grimme et al. [40]. The point group for each geometry was assigned with the help of ORCA's symmetry detection feature. Except for $Li(MeCN)_3^+$, PBE0-D3BJ/def2-TZVP analytical harmonic vibrational frequency calculations for all optimized structures yielded only positive frequencies and consequently, confirmed them as energy minima. In the case of $Li(MeCN)_3^+$, three very small imaginary frequencies ($< 10i\ cm^{-1}$) were obtained, which correspond to the internal rotations of the three methyl groups. As these imaginary frequencies occur independently of the orientation of the methyl groups, they can be regarded as numerical artifacts originating from the very flat potential of the methyl torsion.

Zero-point vibrational energies were determined on the basis of the PBE0-D3BJ/def2-TZVP harmonic vibrational frequencies. Moreover, these frequencies together with the corresponding geometries were used to calculate thermal corrections and entropic contributions according to the ideal gas approximation in combination with Grimme's quasi-RRHO approach [41]. For the calculation of the rotational entropies, the symmetry numbers associated with the assigned point groups of the molecules were applied. The thermochemical corrections were computed at 1.01325 bar and 298.15 K and, in addition, determined at 300 K for Li^+, $Li(A)^+$, $Li(Me_2O)_n^+$ ($n = 2$, 3), and A and at 373 K for Li^+, $Li(A)^+$, and A (A = Me_2O, Et_2O, THF, MeCN). In the case of $Li(MeCN)_n^+$ complexes ($n = 2$, 3), the vibrational modes corresponding to a virtually unhindered methyl torsion (one for $n = 2$ and three for $n = 3$) were treated as free internal rotations within the determination of the thermal corrections and entropic contributions. For this purpose, the program MESMER 4.0 was used [42].

For the optimized structures, single point energies (SPEs) were determined by DLPNO-CCSD(T) calculations [43–45] with the *TightPNO* option. Within these calculations, the frozen core approximation was only used for the elements C and O, because the treatment of core correlation for Li is important for obtaining reliable bond dissociation energies for lithium complexes as highlighted by Rodgers and Armentrout [17]. In line with this procedure, cc-pVQZ basis sets were used for H, C, and O [46] and the core-valence basis set cc-pwCVQZ for Li [47]. For the resolution-of-identity approximation in the DLPNO-CCSD(T) calculations, the auxiliary basis sets cc-pVQZ for H, C, and O [48] and cc-pwCV5Z for Li [49] were employed. For each species, $H°$ and $G°$ values for a certain temperature were obtained by adding the corresponding thermochemical correction from the PBE0-D3BJ/def2-TZVP calculations to the respective DLPNO-CCSD(T) SPE.

In addition, the PBE0-D3BJ geometries of $Li(Et_2O)_n^+$ (n = 2, 3) and Et_2O were re-optimized with the MP2 method [50, 51] with cc-pVTZ basis sets for H, C, and O [46]; the cc-pwCVTZ basis set for Li [47]; and the same frozen core settings as used for the coupled cluster calculations. For the resulting structures, DLPNO-CCSD(T) SPEs were determined as described above.

The XYZ coordinates (in Å) of the optimized structures can be found in the li_complexes_QCC_data.tar file of the Supporting Information.

Results and Discussion

Gas-Phase Reactivity Studies

Exposure of mass-selected $Li(A,B)_2^+$ ions to mixtures of A and B in the gas phase led to the formation of the full series of bis-ligated lithium complexes $Li(A)_2^+$, $Li(A)(B)^+$, and $Li(B)_2^+$ as the result of ligand displacement reactions (Figure 1 for the case of $Li(MeCN)(Me_2O)^+$ subjected to reactions with MeCN and Me_2O). In addition, the tris-ligated complexes $Li(A,B)_3^+$ also appeared and pointed to the occurrence of ligand addition reactions. The absence of any tetra-ligated ions indicates that their stability was too low to permit their formation under the present conditions. It is well-known that the sequential binding energies of alkali metal cations in general and lithium cations in particular decrease as a function of their coordination number [18, 19]. The higher tendency of coordinatively unsaturated Li^+ ions to add ligands was also evident from control experiments on mono-ligated $Li(A)^+$ cations (formed upon collision-induced dissociation of bis-ligated precursor ions), for which addition reactions completely prevailed over ligand displacement reactions. Thus, the present approach could not be used to determine the relative stabilities of mono-ligated $Li(A)^+$ complexes.

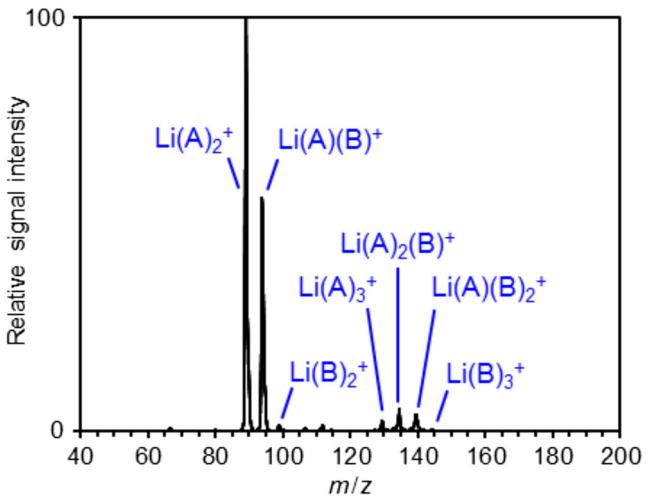

Figure 1. Mass spectrum of mass-selected $Li(A)(B)^+$ and its products formed upon its reaction with a mixture of MeCN (A) and Me_2O (B) for a reaction time of 100 ms

Obviously, the observed ligand displacement reactions of the $Li(A,B)_2^+$ ions did not proceed via a dissociative, but via an associative mechanism, which involved short-lived, energized $Li(A,B)_3^+$ intermediates. These intermediates afforded the products of the ligand displacement reactions by the loss of one ligand. Alternatively, collisions with helium could stabilize the tris-ligated $Li(A,B)_3^+$ complexes, thus explaining the occurrence of ligand addition reactions.

The consideration of all possible ligand displacement and addition reactions as well as ligand dissociation processes interrelating the observed bis- and tris-ligated Li^+ ions results in a complex kinetic scheme (Scheme 2). Note that this scheme does not contain all occurring microscopic elementary steps, such as the collisional stabilization of energized $Li(A,B)_3^+$ intermediates, but only describes the macroscopically observable processes by effective rate constants, which are sufficient for the determination of equilibrium constants.

Due to the significant complexity of the complete network of reactions, we did not attempt to use it as the kinetic model for the fitting but sought to simplify it. We started with a kinetic model including all ligand displacement reactions (described by the rate constants k_{+i}, k_{-i} with i = 1, 2, 9–11) as well as the ligand addition reactions (defined by the rate constants k_{+i} with i = 3–8). The neglect of the ligand dissociation reactions (described by k_{-i} with i = 3–8) seemed valid because the signal intensity of the tris-ligated complexes exhibited a gradual increase and reached high levels only at late reaction times

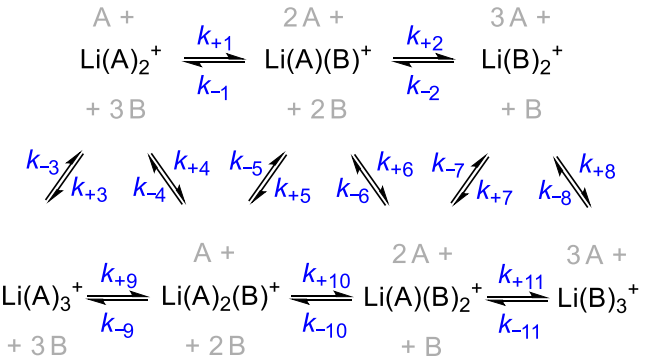

Scheme 2. Complete network of ligand displacement, addition, and dissociation reactions

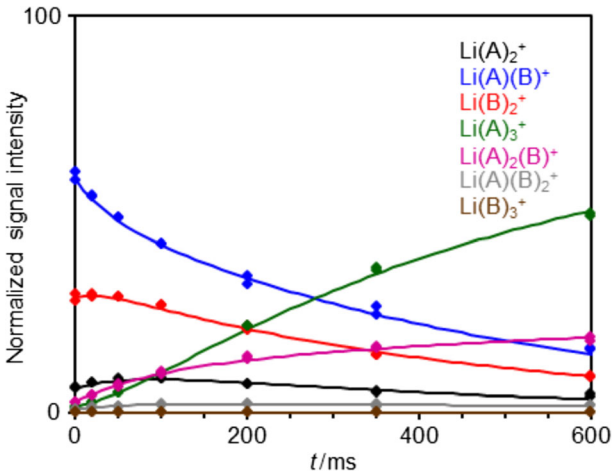

Figure 2. Normalized signal intensities of bis- and tris-ligated lithium ions (diamonds) resulting from the reaction of $Li(A)(B)^+$ with a mixture of A (THF) and B (Et_2O) at different reaction times *t* together with a fit (lines) based on a kinetic model including all ligand displacement and all ligand addition reactions (see text for details)

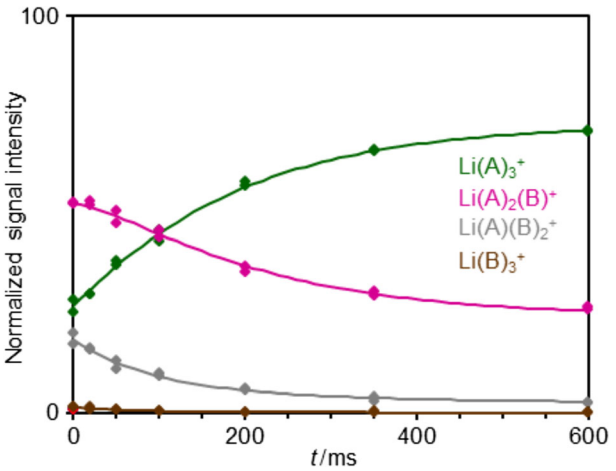

Figure 4. Normalized signal intensities of tris-ligated lithium ions (diamonds) resulting from the reaction of $Li(A)(B)^+$ with a mixture of A (THF) and B (Et_2O) at different reaction times *t* together with a fit (lines) based on a kinetic model considering only ligand displacement reactions of tris-ligated complexes (see text for details)

(Figures 2 and S1, S4, S7, S10, and S13). Indeed, the experimental time profiles could be satisfactorily simulated on the basis of this kinetic model.

However, in several cases, the model turned out to be too flexible with the fitting resulting in multiple solutions, between which could not be easily discriminated and which therefore did not seem suitable for the derivation of reliable equilibrium constants. Therefore, we considered a further simplification of the kinetic model used for the fitting procedure. A characteristic feature of the probed $Li(A,B)_2^+$ and $Li(A,B)_3^+$ systems was the shorter time scale of the ligand displacement than that of the ligand addition reactions. This difference became particularly evident by contrasting it by the behavior of the mono-ligated

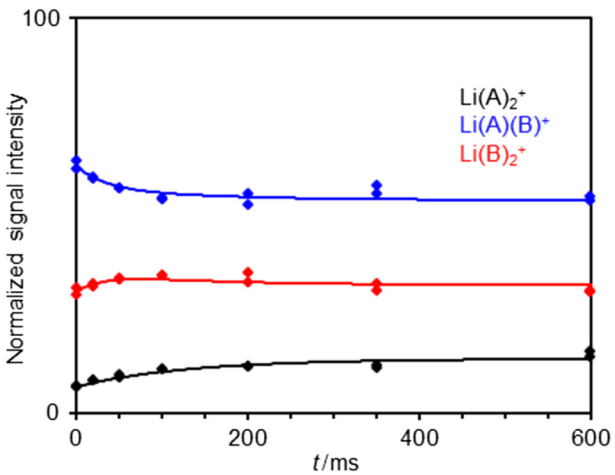

Figure 3. Normalized signal intensities of bis-ligated lithium ions (diamonds) resulting from the reaction of $Li(A)(B)^+$ with a mixture of A (THF) and B (Et_2O) at different reaction times *t* together with a fit (lines) based on a kinetic model considering only ligand displacement reactions of bis-ligated complexes (see text for details)

$Li(A)^+$ ions, which added a further substrate molecule so fast that practically no ligand displacement reactions could be observed (see above). The relative slowness of the ligand addition to the $Li(A,B)_2^+$ ions implies that the equilibration at the level of the bis- and tris-ligated complexes can be treated separately. Accordingly, we divided the complete reaction network into subsets defined by the rate constants k_{+i}, k_{-i} with $i = 1, 2$ for the ligand displacement reactions of $Li(A,B)_2^+$ and $i = 9–11$ for those of $Li(A,B)_3^+$. Plotting of the normalized signal intensities for the bis- and tris-ligated complexes, respectively, showed that in most cases, the equilibration was far advanced or nearly complete within the sampled reaction time (Figures 3 and 4 as well as S2, S3, S5, S6, S8, S9, S11, S12, S14, and S15). This finding implies that the ligand displacement reactions proceeded relatively fast (with rates apparently approaching the order of the collision rate for the exoergic ligand displacement reactions of the bis-ligated complexes) [52, 53]. Fitting of the experimental data to these separate kinetic models furnished reliable and consistent solutions (Tables S1–S6).

From the thus derived rate constants, we calculated equilibrium constants and, ultimately, relative Gibbs reaction energies (Table 1) [54]. In most cases, the obtained values were associated with relatively small uncertainties.

Quantum Chemical Calculations

The calculated structures of the homoleptic $Li(A)_n^+$ complexes [55], $n = 1–3$, clearly show that all ligands probed adopt similar coordination modes, but that they differ in their steric requirements (Figure 5). In particular, $Li(Et_2O)_3^+$ appears to experience steric congestion. We also predicted the sequential ligand dissociation energies of the $Li(A)_3^+$ complexes (Table 2) [56, 57]. Several studies have shown

Table 1. Gibbs Reaction Energies $\Delta G°$ of Ligand Displacements Reactions at $T = 300$ K Derived from the Results of Kinetic Modeling

	$\Delta G°(300\ K)$ (kJ mol^{-1})					
	A = Me_2O/ B = Et_2O	A = Me_2O/ B = THF	A = Me_2O/ B = MeCN	A = Et_2O/ B = THF	A = Et_2O/ B = MeCN	A = THF/ B = MeCN
$Li(A)_2^+ + B \rightarrow Li(A)(B)^+ + A$	− 15.3 ± 1.9	− 16.0 ± 2.5	− 20.2 ± 2.1	− 2.4 ± 0.5	− 6.1 ± 0.2	− 4.8 ± 1.4
$Li(A)(B)^+ + B \rightarrow Li(B)_2^+ + A$	− 11.7 ± 1.6	− 12.9 ± 2.7	− 15.8 ± 1.3	2.2 ± 0.3	− 3.7 ± 0.4	− 2.7 ± 1.5
$Li(A)_3^+ + B \rightarrow Li(A)_2(B)^+ + A$	− 9.7 ± 2.2	− 14.3 ± 4.0	− 18.1 ± 1.5	− 10.5 ± 0.7	− 11.8 ± 0.4	− 5.1 ± 1.4
$Li(A)_2(B)^+ + B \rightarrow Li(A)(B)_2^+ + A$	− 4.6 ± 1.9	− 16.7 ± 4.3	− 14.6 ± 1.2	− 8.0 ± 1.7	− 7.4 ± 0.7	− 2.6 ± 1.6
$Li(A)(B)_2^+ + B \rightarrow Li(B)_3^+ + A$	− 3.5 ± 5.1	− 9.9 ± 3.2	− 10.3 ± 1.3	− 3.6 ± 0.4	− 5.3 ± 0.7	− 1.1 ± 1.6

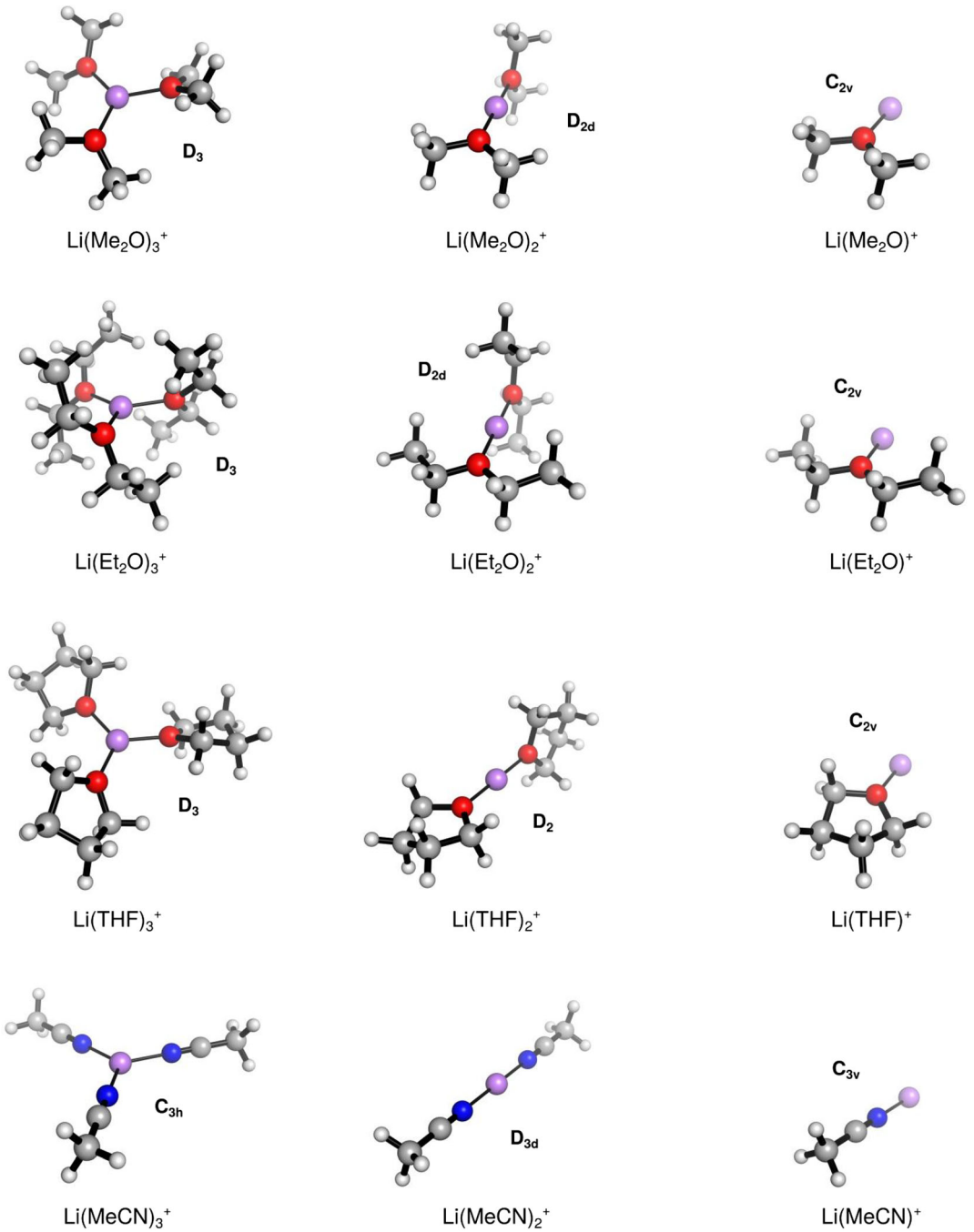

Figure 5. Molecular structures of $Li(A)_n^+$ complexes (A = Me_2O, Et_2O, THF, MeCN; n = 1–3) obtained from PBE0-D3BJ geometry optimizations. The point groups of the geometries are given next to the complexes

Table 2. Electronic Reaction Energies ΔE_{el}, Reaction Enthalpies $\Delta H°$ (for $T = 0$ and 298 K), and Gibbs Reaction Energies $\Delta G°$ (for $T = 298$, 300, and 373 K) for the Ligand Dissociation of $Li(A)_n^+$ Complexes (A = Me_2O, Et_2O, THF, MeCN; $n = 1–3$) Obtained from DLPNO-CCSD(T)//PBE0-D3BJ Calculations in kJ mol^{-1}

	ΔE_{el}	$\Delta H°$ 0 K	$\Delta H°$ 298 K	$\Delta G°$ 298 K	$\Delta G°$ 300 K	$\Delta G°$ 373 K
$Li(Me_2O)^+ \rightarrow Li^+ + Me_2O$	167.3	160.6	162.7	133.8	133.6	126.4
$Li(Me_2O)_2^+ \rightarrow Li(Me_2O)^+ + Me_2O$	138.1	132.4	130.3	91.0	90.7	–
$Li(Me_2O)_3^+ \rightarrow Li(Me_2O)_2^+ + Me_2O$	110.4	104.3	103.0	55.5	55.1	–
$Li(Et_2O)^+ \rightarrow Li^+ + Et_2O$	186.1	180.5	182.2	152.8	152.6	145.0
$Li(Et_2O)_2^+ \rightarrow Li(Et_2O)^+ + Et_2O$	148.5	143.0	140.9	94.8	–	–
$Li(Et_2O)_3^+ \rightarrow Li(Et_2O)_2^+ + Et_2O$	102.0	94.2	93.8	37.8	–	–
$Li(THF)^+ \rightarrow Li^+ + THF$	186.8	179.9	182.3	151.1	150.9	143.2
$Li(THF)_2^+ \rightarrow Li(THF)^+ + THF$	150.2	144.8	142.7	99.8	–	–
$Li(THF)_3^+ \rightarrow Li(THF)_2^+ + THF$	113.7	108.8	106.9	60.3	–	–
$Li(MeCN)^+ \rightarrow Li^+ + MeCN$	185.7	180.6	183.0	153.1	152.9	145.4
$Li(MeCN)_2^+ \rightarrow Li(MeCN)^+ + MeCN$	150.0	145.8	145.1	106.1	–	–
$Li(MeCN)_3^+ \rightarrow Li(MeCN)_2^+ + MeCN$	106.3	102.2	102.7	66.4	–	–

that the applied *TightPNO* DLPNO-CCSD(T) method can nearly reproduce canonical CCSD(T) [58–60]. The latter, commonly referred to as the gold standard of electronic structure theory, allows one to compute relative electronic energies with chemical accuracy when systems are considered that, such as those of the present study, do not require multi-configurational approaches [61]. Given the use of large basis sets and the treatment of core correlation for Li in the present coupled cluster calculations, we estimate the errors of the obtained $\Delta H°$ values to be < 10 kJ mol^{-1}. In line with this estimation, Minenkov et al. reported the dissociation enthalpies of 72 cationic coinage metal complexes calculated by the *NormalPNO* DLPNO-CCSD(T)/cc-pVQZ method to exhibit a mean absolute deviation (MAD) of 9 kJ mol^{-1} from the corresponding experimental results [62]. The additional approximations necessary for the calculation of the $\Delta G°$ values may possibly increase the error of the latter.

The deviation between the computed reaction enthalpy $\Delta H°(0\ K)$ for the dissociation of $Li(Me_2O)^+$ and the corresponding value from guided ion beam measurements [19] amounts to 4.4 kJ mol^{-1} and lies within the experimental uncertainty (Table S7). A similarly good agreement is obtained between the calculated Gibbs reaction energies $\Delta G°(373\ K)$ for the dissociation of $Li(A)^+$, A = Me_2O, Et_2O, THF, and MeCN and the corresponding experimental values [10] (Table S7). This finding lends further support to the ability of the applied computational models to predict accurate LCAs and LCBs for the considered substrates. However, significantly larger discrepancies of 11.8 and 15.5 kJ mol^{-1} occur between the computed and the experimentally determined $\Delta H°(0\ K)$ values for the dissociation of $Li(Me_2O)_2^+$ and $Li(Me_2O)_3^+$, respectively [19] (Table S7). This discrepancy does not necessarily reflect shortcomings in the theoretical methods used in the present study, but could possibly also result from an overestimation of the kinetic shifts operative in the guided ion beam experiments.

Comparison Between Present Experimental and Theoretical Results

We also aimed at a direct comparison between the present experimental and theoretical thermochemical data of homoleptic lithium complexes. As exemplary calculations show, the slight difference in temperature (300 ± 10 K for the experiments and 298 K for the quantum chemical calculations) is insignificant (Table 2).

The Gibbs reaction energies derived from the measurements represent an overdetermined system of linear equations, from which the relative stabilities of the $Li(A)_2^+$ and $Li(A)_3^+$ complexes can be determined (Schemes 3 and S1). The given uncertainties result from the requirement of their overlap with the error bars of the individual Gibbs reaction energies. As references, we choose $Li(Me_2O)_2^+$ and $Li(Me_2O)_3^+$, respectively, because their absolute ligand dissociation enthalpies have been measured and can serve as anchor points for tying up the relative stabilities of the $Li(A)_n^+$ complexes to an

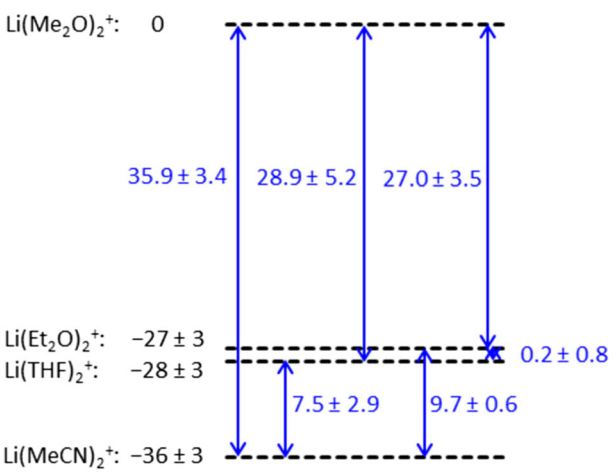

Scheme 3. Relative stabilities of the homoleptic $Li(A)_2^+$ complexes (black) as derived from the measured individual Gibbs reaction energies (blue) at 300 ± 10 K

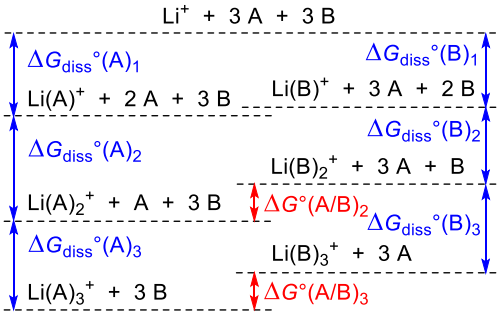

Scheme 4. Thermochemical cycle illustrating the calculation of relative stabilities $\Delta G°(A/B)_n$ from sequential ligand dissociation Gibbs energies $\Delta G_{diss}°$

absolute scale (Table S8). However, as discussed above, the relatively poor agreement between the measured ligand dissociation enthalpies of the $Li(Me_2O)_2^+$ and $Li(Me_2O)_3^+$ ions and the predictions of the present work might be considered a possible caveat against the use of the former as reliable references. Alternatively, the computed ligand dissociation Gibbs energies from the present work could also be used as anchor points.

The combination of the calculated ligand dissociation Gibbs energies $\Delta G°$(298 K) in a simple thermochemical cycle also affords the relative stabilities of the bis- and tris-ligated lithium complexes (Scheme 4). A comparison of the experimental and theoretical values shows an excellent qualitative as well as a good quantitative agreement (MAD = 5.0 kJ mol^{-1}) and, thus, provides additional support for the accuracy of the present results (Table 3). Only for the relative stabilities of $Li(THF)_3^+$, $Li(Et_2O)_2^+$, and $Li(Et_2O)_3^+$, the obtained deviations are larger than the experimental uncertainty. However, even these deviations are still within the estimated accuracy of our computational approach (see above) if the experimental error is taken into account. In all three cases, the calculations underestimate the stability of the complexes. As we have carefully explored the conformational space of the considered species in our computational investigations, we are confident that the underestimation of the stabilities of $Li(THF)_3^+$, $Li(Et_2O)_2^+$, and $Li(Et_2O)_3^+$ is not caused by having missed the global energy minima with respect to $G°$(298 K) [55, 56]. For $Li(Et_2O)_3^+$, which shows the largest discrepancy, we furthermore re-optimized the D_3-symmetric minimum energy structure with the MP2 method, which did not result in a significant geometry change. Likewise, the electronic reaction energy ΔE_{el} for the ligand dissociation of $Li(Et_2O)_3^+$ from DLPNO-CCSD(T)//MP2 calculations (101.9 kJ mol^{-1}) is practically identical to the DLPNO-CCSD(T)//PBE0-D3BJ result. Consequently, there is no indication that the larger discrepancies between the measured and predicted stabilities result from erroneously calculated structures. Alternative possible reasons for the deviations between the experimental and theoretical results are shortcomings in the calculated electronic energies and/or the thermochemical corrections of $Li(THF)_3^+$, $Li(Et_2O)_2^+$, and $Li(Et_2O)_3^+$. As these complexes correspond to the largest species considered in this work, it seems quite plausible that their theoretical description is associated with the largest errors. For the case of $Li(Et_2O)_3^+$ with its rather congested structure, the interplay of steric repulsions and attractive dispersion interactions presumably renders the accurate determination of its electronic energy particularly challenging and, thus, introduces an additional difficulty, with which even the DLPNO-CCSD(T) approach cannot fully cope.

Trends in the Lewis Acidities of Microsolvated Li^+ Ions

Both the present experiments and quantum chemical calculations show that the coordination of ligands to Li^+ ions strongly reduces their Lewis acidity toward further substrate molecules. This finding is in accordance with previous results [18, 19] and mirrors the decrease in positive charge density upon the coordination of Lewis basic ligands. More importantly, the coordination changes not only the absolute binding energies of the ligands but also affects their relative affinities to the lithium center. This effect is most evident in the case of Et_2O. The binding of a single Et_2O molecule to Li^+ is energetically comparable to that of a single THF molecule, but significantly more favorable than that of a single Me_2O molecule (Table 2). The situation changes completely for the tris-ligated complexes. Here, $Li(Et_2O)_3^+$ is destabilized to such an extent that it loses one ligand even more easily than its $Li(Me_2O)_3^+$ counterpart. Most likely, this peculiar behavior results from the higher steric demands of the Et_2O ligand. While being of no consequence for complexes in low coordination states, they cause substantial steric congestion in the tris-ligated system (Figure 5). An analysis of the ligand displacement reactions also shows that the coordination of a given ligand to the lithium center modulates the affinity of the latter to another one (Table 1). If $Li(A)_2^+$ undergoes reactions with a substrate B that is more Lewis basic than A, the first ligand displacement in almost all cases has a stronger effect than the second one. An

Table 3. Comparison of the Measured and Theoretically Predicted Stabilities of Bis- and Tris-Ligated Lithium Complexes $Li(A)_2^+$ and $Li(A)_3^+$ Relative to $Li(Me_2O)_2^+$ and $Li(Me_2O)_3^+$, respectively

A	$\Delta G°(Li(A)_2^+)$ (kJ mol^{-1})		Δ	$\Delta G°(Li(A)_3^+)$ (kJ mol^{-1})		Δ
	Experiment	Theory		Experiment	Theory	
Me_2O	0	0	0	0	0	0
Et_2O	−27 ± 3	−22.9	4.1	−18 ± 4	−5.2	12.8
THF	−28 ± 3	−26.2	1.8	−39 ± 4	−31.0	8.0
MeCN	−36 ± 3	−34.4	1.6	−44 ± 4	−45.3	−1.3

analogous trend can be discerned for the tris-ligated complexes. Presumably, this behavior reflects changes in the charge densities of the lithium center in the different complexes. With an increasing number of more Lewis basic ligands bound to the metal, its positive charge density is diminished, which in turn renders the effect of further ligand displacement reactions less conspicuous.

Conclusion

As the present study has shown, the coordination of ligands to Li^+ exerts significant effects on the affinity of the latter toward further Lewis basic substrates. The most obvious trend is the decrease of ligand binding energies as a function of the coordination number. This behavior can be simply rationalized by the gradual saturation of the positive charge density at the Li^+ center with an increasing number of ligands. At the same time, more subtle and less foreseeable effects can occur as demonstrated by the case of $Li(Et_2O)_n^+$. While mono-ligated $Li(Et_2O)^+$ behaves in a normal way and exhibits a stronger ligand binding than $Li(Me_2O)^+$, the higher steric demands of Et_2O lead to a destabilization of the tris-ligated $Li(Et_2O)_3^+$ complex, which, thus, undergoes ligand dissociation more easily than its $Li(Me_2O)_3^+$ analog. This example clearly shows that microsolvation can significantly change gas-phase lithium cation basicities.

Furthermore, the present study provides a set of experimental thermochemical data, which can serve as a benchmark for assessing the reliability of quantum chemical calculations on (micro)solvated lithium ions. The good agreement achieved between the measured and computed quantities points to the suitability of the computational methods applied in this work. Nevertheless, the examples of $Li(THF)_3^+$, $Li(Et_2O)_2^+$, and $Li(Et_2O)_3^+$ highlight remaining difficulties associated with the accurate calculation of ligand dissociation Gibbs energies by state-of-the-art approaches.

Acknowledgements

We gratefully acknowledge the financial support by the Deutsche Forschungsgemeinschaft (DFG, German Research Foundation) − 389479699/GRK2455.

References

1. Snieckus, V.: Directed ortho metalation. Tertiary amide and O-carbamate directors in synthetic strategies for polysubstituted aromatics. Chem. Rev. **90**, 879–933 (1990)
2. Phiel, C.J., Klein, P.S.: Molecular targets of lithium action. Ann. Rev. Pharm. Toxicol. **41**, 789–813 (2001)
3. Whittingham, M.S.: Lithium batteries and cathode materials. Chem. Rev. **104**, 4271–4302 (2004)
4. Galiano-Roth, A.S., Collum, D.B.: Structure and reactivity of lithium diisoproplyamide (LDA). The consequences of aggregation and solvation during the metalation of an N,N-dimethylhydryzone. J. Am. Chem. Soc. **111**, 6772–6778 (1989)
5. John, M., Auel, C., Behrens, C., Marsch, M., Harms, K., Bosold, F., Gschwind, R.M., Rajamohanan, P.R., Boche, G.: The relation between ion pair structures and reactivities of lithium cuprates. Chem. Eur. J. **6**, 3060–3068 (2000)
6. Nakamura, E., Mori, S.: Wherefore art thou copper? Structures and reaction mechanisms of organocuprate clusters in organic chemistry. Angew. Chem. Int. Ed. **39**, 3750–3771 (2000)
7. Yoshikai, N., Nakamura, E.: Mechanisms of nucleophilic organocopper(I) reactions. Chem. Rev. **112**, 2339–2372 (2011)
8. Woodin, R.L., Beauchamp, J.L.: Binding of lithium(1+) ion to Lewis bases in the gas phase. Reversals in methyl substituent effects for different reference acids. J. Am. Chem. Soc. **100**, 501–508 (1978)
9. Herreros, M., Gal, J.-F., Maria, P.-C., Decouzon, M.: Gas-phase basicity of simple amides toward proton and lithium cation: an experimental and theoretical study. Eur. J. Mass Spectrom. **5**, 259–269 (1999)
10. Burk, P., Koppel, I.A., Koppel, I., Kurg, R., Gal, J.-F., Maria, P.-C., Herreros, M., Notario, R., Abboud, J.-L.M., Anvia, F., Taft, R.W.: Revised and expanded scale of gas-phase lithium cation basicities. An experimental and theoretical study. J. Phys. Chem. A. **104**, 2824–2833 (2000)
11. Irigoras, A., Mercero, J.M., Silanes, I., Ugalde, J.M.: The ferrocene −lithium cation complex in the gas phase. J. Am. Chem. Soc. **123**, 5040–5043 (2001)
12. Feng, W.J., Gronert, S., Lebrilla, C.: The lithium cation binding energies of gaseous amino acids. J. Phys. Chem. A. **107**, 405–410 (2003)
13. Gal, J.-F., Maria, P.-C., Mò, O., Yáñez, M., Kuck, D.: Complexes between lithium cation and diphenylalkanes in the gas phase: the pincer effect. Chem. Eur. J. **12**, 7676–7683 (2006)
14. Gal, J.-F., Maria, P.-C., Decouzon, M., Mó, O., Yáñez, M.: Gas-phase lithium-cation basicities of some benzene derivatives: an experimental and theoretical study. Int. J. Mass Spectrom. **219**, 445–456 (2002)
15. Hallmann, M., Raczyńska, E.D., Gal, J.-F., Maria, P.-C.: Gas-phase lithium cation basicity of histamine and its agonist 2-(β-aminoethyl)-pyridine: experimental (FT-ICR-MS) and theoretical studies (DFT) of chelation effect. Int. J. Mass Spectrom. **267**, 315–323 (2007)
16. Rodgers, M.T., Armentrout, P.B.: Cationic noncovalent interactions: energetics and periodic trends. Chem. Rev. **116**, 6542–5687 (2016)
17. Rodgers, M.T., Armentrout, P.B.: A critical evaluation of the experimental and theoretical determination of lithium cation affinities. Int. J. Mass Spectrom. **267**, 167–182 (2007)
18. Dzidic, I., Kebarle, P.: Hydration of the alkali ions in the gas phase. Enthalpies and entropies of reactions $M^+(H_2O)_{n-1} + H_2O = M^+(H_2O)_n$. J. Phys. Chem. **74**, 1466–1474 (1970)
19. More, M.B., Glendening, E.D., Ray, D., Feller, D., Armentrout, P.B.: Cation–ether complexes in the gas phase: bond dissociation energies and equilibrium structures of $Li^+[O(CH_3)_2]_x$, x = 1–4. J. Phys. Chem. **100**, 1605–1614 (1996)
20. Koszinowski, K., Böhrer, P.: Aggregation and reactivity of organozincate anions probed by electrospray mass spectrometry. Organometallics. **28**, 100–110 (2009)
21. Putau, A., Koszinowski, K.: Association and dissociation of lithium cyanocuprates in ethereal solvents. Organometallics. **30**, 4771–4778 (2011)
22. Koszinowski, K.: Oxidation state, aggregation, and heterolytic dissociation of allyl indium reagents. J. Am. Chem. Soc. **132**, 6032–6040 (2010)
23. Putau, A., Koszinowski, K.: Probing cyanocuprates by electrospray ionization mass spectrometry. Organometallics **29**, 3593-3601 (2010); addition/correction. Organometallics. **29**, 6841–6842 (2010)
24. Parchomyk, T., Koszinowski, K.: Substitution reactions of gaseous ions in a three-dimensional quadrupole ion trap. J. Mass Spectrom. **54**, 81–87 (2019)
25. Gronert, S.: Estimation of effective ion temperatures in a quadrupole ion trap. J. Am. Soc. Mass Spectrom. **9**, 845–848 (1998)
26. Gronert, S., Pratt, L.M., Mogali, S.: Substituent effects in gas-phase substitutions and eliminations: β-halo substituents. Solvation reverses S_N2 substituent effects. J. Am. Chem. Soc. **123**, 3081–3091 (2001)
27. Waters, T., O'Hair, R.A.J., Wedd, A.G.: Catalytic gas phase oxidation of methanol to formaldehyde. J. Am. Chem. Soc. **125**, 3384–3396 (2003)
28. Mendes, P.: GEPASI: a software package for modelling the dynamics, steady states and control of biochemical and other systems. Comput. Applic. Biosci. **9**, 563–571 (1993)
29. Mendes, P.: Biochemistry by numbers: simulation of biochemical pathways with Gepasi 3. Trends Biochem. Sci. **22**, 361–363 (1997)
30. Mendes, P., Kell, D.B.: Non-linear optimization of biochemical pathways: applications to metabolic engineering and parameter estimation. Bioinformatics. **14**, 869–883 (1998)

31. Gioumousis, G., Stevenson, D.P.: Reactions of gaseous molecule ions with gaseous molecules. V. Theory. J. Chem. Phys. **29**, 294–299 (1958)
32. For the experiments with Me_2O/THF, only two out of the four measurements afforded reliable results
33. Neese, F.: The ORCA program system. Wiley Interdiscip. Rev.: Comput. Mol. Sci. **2**, 73–78 (2012)
34. Neese, F.: Software update: the ORCA program system, version 4.0. Wiley Interdiscip. Rev.: Comput. Mol. Sci. (2018). https://doi.org/10.1002/wcms.1327
35. ORCA, version 4.0; Max Planck Institute for Chemical Energy Conversion: Mülheim a. d. Ruhr, Germany (2017)
36. Adamo, C., Barone, V.: Toward reliable density functional methods without adjustable parameters: the PBE0 model. J. Chem. Phys. **110**, 6158–6170 (1999)
37. Grimme, S., Antony, J., Ehrlich, S., Krieg, H.: A consistent and accurate ab initio parametrization of density functional dispersion correction (DFT-D) for the 94 elements H-Pu. J. Chem. Phys. **132**, 154104 (2010)
38. Grimme, S., Ehrlich, S., Goerigk, L.: Effect of the damping function in dispersion corrected density functional theory. J. Comput. Chem. **32**, 1456–1465 (2011)
39. Weigend, F., Ahlrichs, R.: Balanced basis sets of split valence, triple zeta valence and quadruple zeta valence quality for H to Rn: design and assessment of accuracy. Phys. Chem. Chem. Phys. **7**, 3297–3305 (2005)
40. Grimme, S., Brandenburg, J.G., Bannwarth, C., Hansen, A.: Consistent structures and interactions by density functional theory with small atomic orbital basis sets. J. Chem. Phys. **143**, 054107 (2015)
41. Grimme, S.: Supramolecular binding thermodynamics by dispersion-corrected density functional theory. Chem. Eur. J. **18**, 9955–9964 (2012)
42. Glowacki, D.R., Liang, C.-H., Morley, C., Pilling, M.J., Robertson, S.H.: MESMER: an open-source master equation solver for multi-energy well reactions. J. Phys. Chem. A. **116**, 9545–9560 (2012)
43. Riplinger, C., Neese, F.: An efficient and near linear scaling pair natural orbital based local coupled cluster method. J. Chem. Phys. **138**, 034106 (2013)
44. Riplinger, C., Sandhoefer, B., Hansen, A., Neese, F.: Natural triple excitations in local coupled cluster calculations with pair natural orbitals. J. Chem. Phys. **139**, 134101 (2013)
45. Riplinger, C., Pinski, P., Becker, U., Valeev, E.F., Neese, F.: Sparse maps—a systematic infrastructure for reduced-scaling electronic structure methods. II. Linear scaling domain based pair natural orbital coupled cluster theory. J. Chem. Phys. **144**, 024109 (2016)
46. Dunning Jr., T.H.: Gaussian basis sets for use in correlated molecular calculations. I. The atoms boron through neon and hydrogen. J. Chem. Phys. **90**, 1007–1023 (1989)
47. Prascher, B.P., Woon, D.E., Peterson, K.A., Dunning Jr., T.H., Wilson, A.K.: Gaussian basis sets for use in correlated molecular calculations. VII. Valence, core-valence, and scalar relativistic basis sets for Li, Be, Na, and Mg. Theor. Chem. Acc. **128**, 69–82 (2011)
48. Weigend, F., Köhn, A., Hättig, C.: Efficient use of the correlation consistent basis sets in resolution of the identity MP2 calculations. J. Chem. Phys. **116**, 3175–3183 (2002)
49. Hättig, C.: Optimization of auxiliary basis sets for RI-MP2 and RI-CC2 calculations: core–valence and quintuple-ζ basis sets for H to Ar and QZVPP basis sets for Li to Kr. Phys. Chem. Chem. Phys. **7**, 59–66 (2005)
50. Møller, C., Plesset, M.S.: Note on an approximation treatment for many-electron systems. Phys. Rev. **46**, 618–622 (1934)
51. Szabo, A., Ostlund, N.S.: Modern quantum chemistry: introduction to advanced electronic structure theory, pp. 350–353. Dover Publications, New York (1996)
52. Chesnavich, W., Su, T., Bowers, M.T.: Collisions in a noncentral field: a variational and trajectory investigation of ion-dipole capture. J. Chem. Phys. **72**, 2641–2655 (1980)
53. As explained in the Experimental Section, the fitting procedure determined reliable ratios of bimolecular rates constants, but no reliable individual absolute rate constants
54. An alternative way to determine the relative stabilities of $Li(A,B)_2^+$ complexes would compare the relative rates of the different fragmentation reactions of heteroleptic $Li(A,B)_3^+$ complexes upon energetic collisions (so-called kinetic method): Cooks, R. G., Wong, P. S. H.: Kinetic method of making thermochemical determinations: advances and applications. Acc. Chem. Res. **31**, 379–386 (1998)
55. For the $Li(THF)_3^+$ complex, two D_3-symmetric diastereomers were identified, which differ significantly with respect to their electronic energy. As the electronically less stable diastereomer features a lower $G°$(298 K) value, only this structure is considered in Figure 5 and within the calculation of dissociation energies (for details, see Figure S16)
56. For the calculation of sequential ligand dissociation energies of the $Li(Et_2O)_3^+$ complex, we have only considered the *trans-trans* conformation of Et_2O because, in agreement with previous experimental studies [57], our calculations predict this conformation to be the most stable one. Similarly, $Li(Et_2O)_n^+$ complexes (n = 1–3) featuring one *trans-gauche* Et_2O ligand turned out to be less stable than or, in case of (n = 3), equally stable as the complexes with only *trans-trans* Et_2O ligands. Consequently, we have used only the latter for the calculation of dissociation energies (for details, see Figure S17)
57. Kuze, N., Kuroki, N., Takeuchi, H., Egawa, T., Konaka, S.: Structural and conformational analysis of diethyl ether by molecular orbital constrained electron diffraction combined with microwave spectroscopic data. J. Mol. Struct. **301**, 81–94 (1993)
58. Sparta, M., Neese, F.: Chemical applications carried out by local pair natural orbital based coupled-cluster methods. Chem. Soc. Rev. **43**, 5032–5041 (2014)
59. Liakos, D.G., Sparta, M., Kesharwani, M.K., Martin, J.M.L., Neese, F.: Exploring the accuracy limits of local pair natural orbital coupled-cluster theory. J. Chem. Theory Comput. **11**, 1525–1539 (2015)
60. Minenkov, Y., Bistoni, G., Riplinger, C., Auer, A.A., Neese, F., Cavallo, L.: Pair natural orbital and canonical coupled cluster reaction enthalpies involving light to heavy alkali and alkaline earth metals: the importance of sub-valence correlation. Phys. Chem. Chem. Phys. **19**, 9374–9391 (2017)
61. Helgaker, T., Jørgensen, P., Olsen, J.: Molecular electronic structure theory, 1st edn. Wiley & Sons, Ltd., West Sussex (2000)
62. Minenkov, Y., Chermak, E., Cavallo, L.: Accuracy of DLPNO–CCSD(T) method for noncovalent bond dissociation enthalpies from coinage metal cation complexes. J. Chem. Theory Comput. **11**, 4664–4676 (2015)